

Article

Fluorescence-Based Image Analysis of Seepage Behavior in Drip Irrigation: Exploring Varied Fractal Grading in Media Permeability

Xiaolong Wang^{1,2}, Junjie Huang^{1,2}, Xiang Li^{1,2}, Wenbin Yuan^{1,2}, Hongchang Liu^{1,2} , Min Gan^{1,2}, Jun Wang^{1,2} and Yansheng Zhang^{1,2,*}

¹ School of Minerals Processing & Bioengineering, Central South University, Changsha 410083, China; 215612089@csu.edu.cn (X.W.)

² Key Laboratory of Biohydrometallurgy of Ministry of Education, Central South University, Changsha 410083, China

* Correspondence: yanshengzhang_csu@126.com

Abstract: In the recycling of low-value metallic elements, heap leaching is commonly employed. The particle size distribution is a crucial parameter in heap leaching implementation, and the percolation behavior of a heap has always been a focal point in heap leaching technology. This paper utilizes a novel form of ultraviolet fluorescence image acquisition and fluorescence image analysis to investigate the percolation process with different fractal dimension particle size distributions, where the maximum particle diameter is 10 mm. The ore used was low-grade copper ore. The results indicate that the new fluorescence image analysis method can reveal different percolation regions during the heap leaching process, aiding in a better understanding of heap leaching behavior. The combined study found that under irrigation conditions of 10 mL/min, seepage was more uniform under the heap structure formed by a particle gradation with a fractal dimension of 2.2.

Keywords: heap leaching; UV fluorescence; particle size distribution; seepage; fractal dimension



Citation: Wang, X.; Huang, J.; Li, X.; Yuan, W.; Liu, H.; Gan, M.; Wang, J.; Zhang, Y. Fluorescence-Based Image Analysis of Seepage Behavior in Drip Irrigation: Exploring Varied Fractal Grading in Media Permeability. *Minerals* **2024**, *14*, 482. <https://doi.org/10.3390/min14050482>

Academic Editor: Luis A. Cisternas

Received: 19 February 2024

Revised: 26 March 2024

Accepted: 28 March 2024

Published: 30 April 2024



Copyright: © 2024 by the authors. Licensee MDPI, Basel, Switzerland. This article is an open access article distributed under the terms and conditions of the Creative Commons Attribution (CC BY) license (<https://creativecommons.org/licenses/by/4.0/>).

1. Introduction

Heap leaching, a cost-effective hydrometallurgical technique, is widely applied in the extraction of low-grade ores such as gold and copper [1,2]. Unlike other hydrometallurgical processes, heap leaching requires attention to the flow of water within the heap. Within the heap structure, water serves as a crucial medium for mineral dissolution and reactions, significantly influencing the internal reactions within the ore heap [3]. Different structures within the heap result in distinct forms of water flow [4]. The complex dual-porosity structure of the heap, consisting of gaps between ore particles and internal pores within the ore, adds complexity to the water flow phenomena within the heap [5]. For heaps without agglomeration, there are numerous factors determining the pore structure, and particle size distribution is one of the most significant factors [6].

When studying heap leach particle size distributions, various indicators such as grading curves, maximum particle diameters, and the coefficient of uniformity are often employed to describe the grading of a heap [7,8]. However, for precise control of heap leaching, accurate description of the crushed ore gradation is essential. The aforementioned methods require the synthesis of multiple parameters to accurately describe the specific crushed ore gradation, increasing the difficulty of gradation analysis. Using fractal description of the crushed ore gradation can effectively address this issue, as it enables precise description of particle size distribution through fractal dimension. Self-similarity and fractals are objective characteristics of many natural phenomena, and some minerals exhibit fractal patterns after fragmentation [9,10]. In 1992, Tyler and Wheatcraft first used fractals to describe soil particle grading [11,12]. Ding et al. also established a kinetic model

for uranium heap leaching using fractal dimensions [13]. Studying leachate flow in heap structures with fractal grading provides a closer representation of the actual heap leaching production process. Here is a brief explanation of fractals and how they are used to describe grading.

According to the definition of fractals [11], the relationship between the quantity of mineral particles and their characteristic scales, satisfying a certain power law correlation, can be termed as exhibiting fractal characteristics. The equation is as follows:

$$N(r > R) \propto R^{-D} \quad (1)$$

N represents the number of particles with characteristic scales r greater than R , where D is the fractal dimension of the particle distribution, and R is a specified characteristic scale for comparison. However, counting the number of particles is impractical when analyzing the particle size distribution. Therefore, a power law relationship between the mass of particles and sieve diameter is used as a substitute. In earlier studies, Turcotte derived the fractal relationship for particle distribution based on the power law between particle mass and sieve diameter. Subsequently, Tyler et al. employed a three-dimensional box-counting method, deriving the same fractal relationship while preserving strict similarities between particle quantity and size [12,14]. The final fractal relationship between mass and sieve diameter is expressed by the following equation:

$$\frac{M(r < R)}{M_T} = \left(\frac{R}{R_L}\right)^{3-D} \quad (2)$$

$M(r < R)$ represents the mass of particles with diameters smaller than a specific size R ; M_T is the total mass of particles; R is the specified particle size (corresponding to the sieve diameter); and R_L is the maximum particle diameter.

In the heap leaching system, the unsaturated flow of liquid within the heap remains highly intricate. Numerous researchers have employed different methods to study the hydrological processes in heaps, and many have adopted visualization techniques for studying heap leach percolation. These methods include direct observation of moist regions [15,16], magnetic resonance imaging (MRI) [17], and X-ray computed tomography (X-CT) for characterizing fluid flow within the heap [18]. Some researchers have utilized high-resolution positron emission tomography (PET) to characterize fluid changes within the heap [2]. UV-excited fluorescence dye imaging is also a simple and effective method for studying hydrological processes within heaps. Ilankoon successfully explored the flow of liquid between ore particles using fluorescent labeling imaging [19]. As in the aforementioned research methods, current UV-excited fluorescence dye imaging approaches have not been able to monitor the ongoing flow of liquid in previously marked regions.

This study refined the method of UV fluorescence excitation imaging for investigating percolation by incorporating image analysis of subsequent fluorescence marker washing processes. This enhancement provides further insights into the liquid diffusion patterns in subsequent fine-grained, wet mineral beds. Simultaneously, a new approach has been employed to examine the percolation process in heaps that closely resemble the particle size distribution of crushed ores. The findings of this research aim to contribute to a more comprehensive understanding of the heap leaching percolation mechanisms for low-grade crushed ores, providing valuable insights for practical heap leaching operations.

2. Materials and Methods

2.1. Experimental Setup

The main body of the entire experimental setup was a two-dimensional organic glass column, 40 cm in length, 30 cm in height, and 5 cm in thickness, as illustrated in Figure 1. Seventeen semicylindrical liquid collection outlets were uniformly arranged at the bottom of the two-dimensional column and connected through conduits to plastic bottles below to monitor changes in water flow. The central collection outlet is marked as number 0, and

those to the left, facing the camera, are labeled from -1 to -8 , while those to the right are labeled from 1 to 8 , following a setup similar to that of Ilankoon et al. [19].

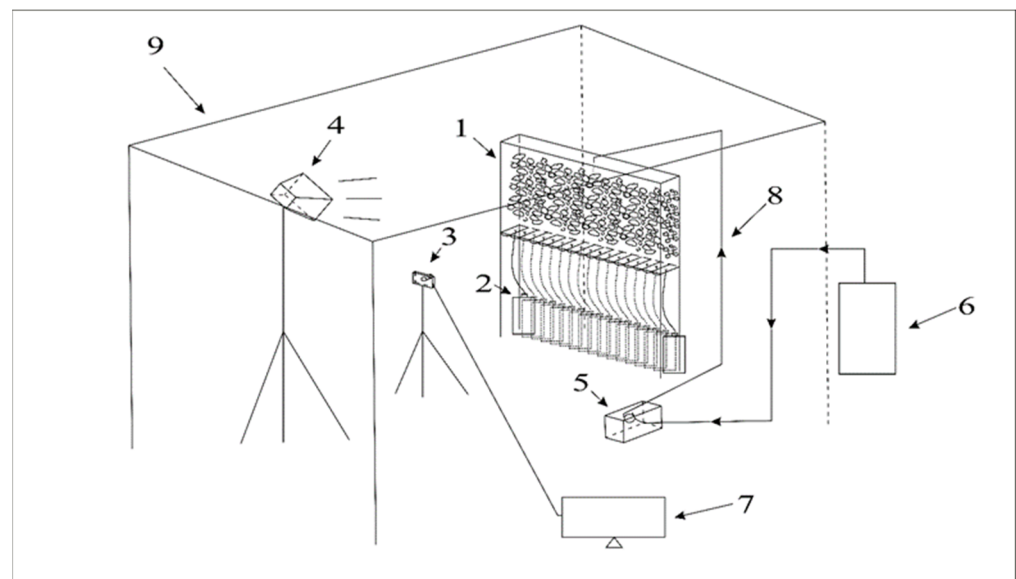


Figure 1. Experimental setup for fluorescence leachate monitoring. 1—Pseudo2-D column, 2—Liquid collection bottle, 3—Camera, 4—Square UV light cup, 5—Peristaltic pump, 6—Liquid storage tank, 7—Monitor, 8—Pipelines, 9—Light shield.

To maintain a dark environment for convenient filming, a stable darkroom was constructed for the experiment. A cup-shaped UV light with a power of 40 W and a wavelength of 365 nm was utilized as the sole light source to excite fluorescence. Unlike in UV light tubes, a square-shaped light cup concentrates and evenly distributes ultraviolet light, avoiding the occurrence of reflective spots during the irradiation process. The camera sensor used for image acquisition has a size of $1/2.3''$, an effective pixel count of 12 million, and pixel dimensions of $1.55 \mu\text{m} \times 1.55 \mu\text{m}$. To minimize errors caused by variations in fluorescence intensity due to differences in distances from the light, the camera, the two-dimensional column, and the irradiation light were fixed at specific distances. Calculations show that each pixel in the captured images represents an actual size of approximately $60 \mu\text{m}$, allowing for precise recording of changes in liquid penetration within the ore heap.

2.2. Materials

The ore used in this study was sourced from the Dexing copper mine and is constituted by low-grade chalcopyrite ore with a density (ρ) of 2.64 g/cm^3 and an internal porosity of approximately 2%. The main components of the ore are quartz, pyrite, mica, etc. Nine groups of ore particles with sizes ranging from 10–8 mm, 8–6 mm, 6–5 mm, 5–3 mm, 3–1.6 mm, 1.6–1 mm, 1–0.6 mm, 0.6–0.3 mm, and <0.3 mm were selected. Fractal equations (Equation (2)) were employed to establish gradations with fractal dimensions of 1.6, 1.8, 2.0, 2.2, and 2.4. The logarithmic distribution curves of fractal particle sizes are shown in Figure 2. For each set of graded ores, the total weight was 8.0 kg. The height of each heap, as measured from images, is presented in Table 1. The thickness of the columns is five times the maximum particle size, aiming to minimize the impact of column thickness on particle accumulation and effectively showcase the liquid infiltration process. To maintain uniformity in heap formation and ensure good repeatability, and to adequately demonstrate the infiltration characteristics of each gradation, the ore was sampled multiple times using a quartering method during heap filling, dividing it into sixteen equal portions, which were slowly and evenly filled into the two-dimensional column.

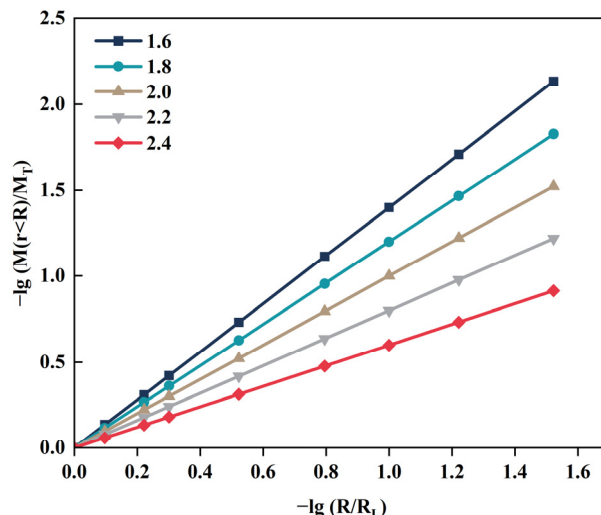


Figure 2. Double logarithmic plot of the fractal distribution of particle size for five ore samples.

Table 1. Stack heights of five sets of samples.

Fractal dimension	1.6	1.8	2	2.2	2.4
Pile height (cm)	24.1	23.4	23.1	22.5	22.1

The tracer used in the experiment was sodium fluorescein, which has minimal environmental impact [20]. The concentration of the solution was set at 1.0 g/L (after comparison, under these conditions, the diffusion process of the fluorescent liquid and the subsequent washing process could be well observed). Image processing and calculations were performed using the software ImageJ 1.53q.

2.3. Experimental Procedure

A complete permeation experiment lasted for 600 min. The first 300 min involved drip irrigation with a sodium fluorescein solution, followed by the next 300 min of irrigation with water. The peristaltic pump was set to deliver a liquid irrigation rate of 10 mL/min. After the first 300 min of irrigation, the fluorescein solution nearly covered the entire plane. In the subsequent 300 min with water irrigation, the decrease in fluorescence intensity was observed to further study the changes in leachate flow within the moist ore bed. Liquid weights collected from the collection outlet will be recorded every 300 min (completing one stage) during the permeation process. The camera captured images of the heap every minute once the permeation experiment began. Due to the large number of images captured, representative results were selected based on image characteristics for presentation and discussion.

2.4. Image Analysis

Due to the retention of fine particles, the fluorescent solution was able to flow through the abundant pores, and the liquid diffusion outside and inside the particles did not differ much in the experiments, so that the visible wetting region basically overlapped with the fluorescent region. For the wet pictures of the first 300 min of the ore pile, the boundaries between wet and unwetted areas were distinguished to simplify the picture information, as shown in Figure 3.

In photos taken during the second 300 min, interference from surrounding fluorescence makes the observation of the percolation area challenging. To facilitate the observation and computation of the percolation area, we performed a subtraction operation using the fluorescence image before water addition from the images captured after water addition. This process generates a clear percolation image of the wet mineral bed, referred to as the

‘fluorescence-subtracted image’. The result is illustrated in Figure 4. This image serves as the analytical representation of liquid flow within the moist ore bed. In comparison to images obtained by dripping only fluorescein solution, these images contained more specific material exchange information within the heap and depict the flow conditions more accurately.

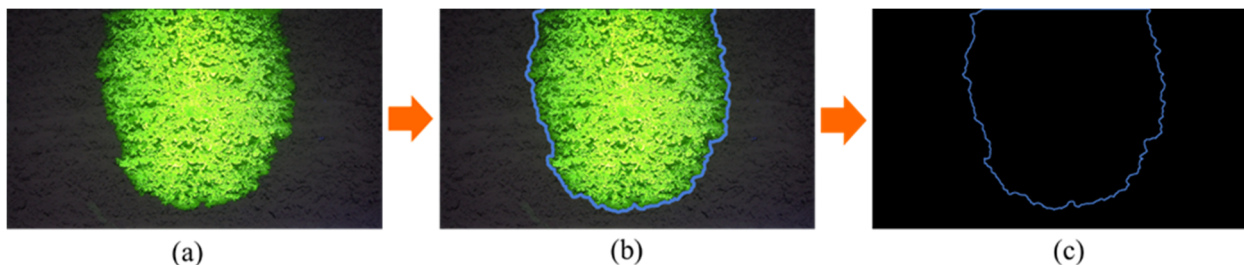


Figure 3. Original image (a); extracted image edges of wetted areas (b); plotted wetting profile of mineralized piles (c).

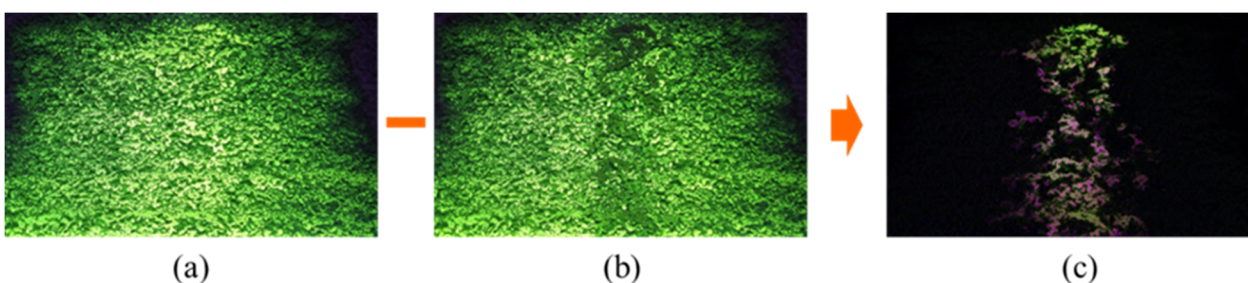


Figure 4. The fluorescence subtraction image at 10 min in the second stage (c) was obtained by subtracting the image at 10 min in the second stage (b) from the fluorescence image at 300 min (a).

3. Results and Discussion

3.1. Liquid Moistening Characteristics in Dry Ore Heap

Based on the moistening characteristics, boundary processing was applied to images at different time points in the heap, as shown in Figure 5. The wet edge curves from the inside to the outside represent changes in the moistened area of the ore bed over time.

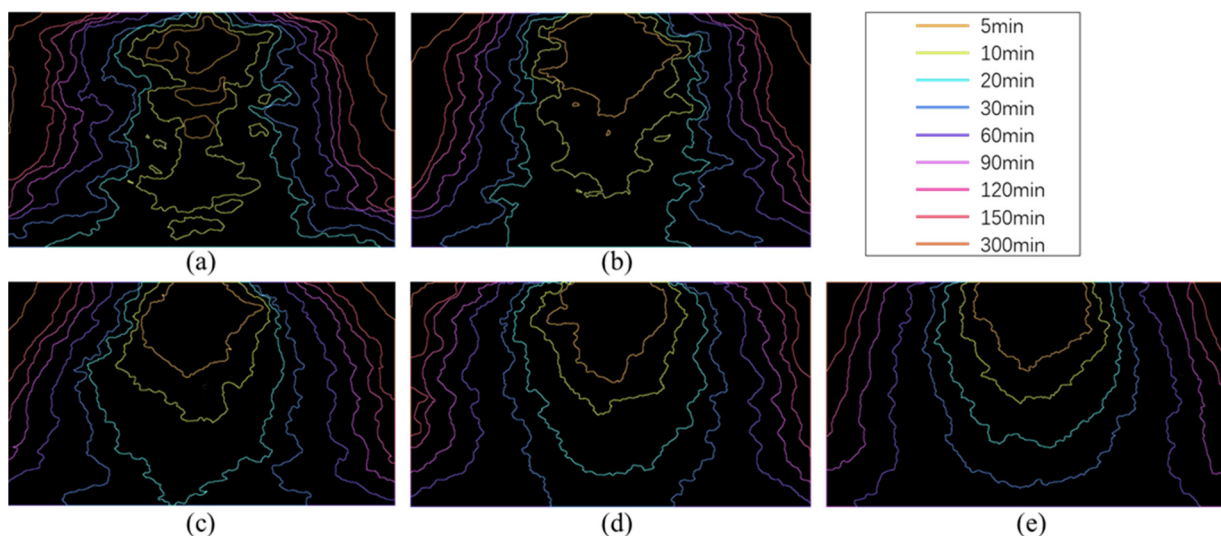


Figure 5. Wetting curves of the ore body with fractal dimensions of 1.6–2.4 (a–e) during the first 300 min.

Figure 5 indicates that the liquid gradually moistens the heap starting from the drip point, and by the 300th min, the heap is essentially wetted by the fluorescent solution. Dry areas of the heap are concentrated in the upper two corners of the heap and decrease with an increase in fractal dimension. As the fractal dimension increases, the proportion of fine particles in the heap also increases, enhancing capillary action in the entire dry ore bed, allowing more solution to fill the interstices between ore particles [21,22]. When the interior of the ore is filled with liquid, it facilitates the diffusion and transport of solutes, thereby enhancing internal mass transfer processes. However, mass transfer within a heap is not only diffusion but also involves the consideration of liquid convection [23]. Therefore, an examination of the actual flow regions within the heap is necessary, and this will be discussed in detail in Section 3.3.

To quantitatively understand the wetting process of the dry ore bed, the percentage of moistened area at different time points was calculated, as shown in Figure 6a. The wetted area of the heaps grows rapidly in the early stages and slows down in the later stages. Combining this information with Figure 5, in the early stages, the vertical expansion of the wetted area for all heaps leads to a rapid increase in the moistened area. When the wetted area reaches the bottom, the increase in the moistened area is gradually dominated by lateral capillary action, becoming slower. The extent of lateral extension of the moistened area after 60 min for different time points is represented by the ratio of the wetted area to the heap height, as shown in Figure 6b. After 90 min, heaps with fractal dimensions of 2.2 and 2.4 exhibit similar lateral wetting trends, indicating that the promoting effect of capillary action on the final wetting extent of the heap is limited under a certain irrigation intensity. At 60 min, the lateral diffusion extent of the heap with a fractal dimension of 2.4 is only slightly higher than that of 1.6. This may be attributed to an increase in the proportion of fine particles to a certain extent, leading to an increased amount of capillary water in the pores within and between particles. As a result, more time is needed for the excess capillary channels to be filled, thereby inhibiting the initial lateral wetting rate.

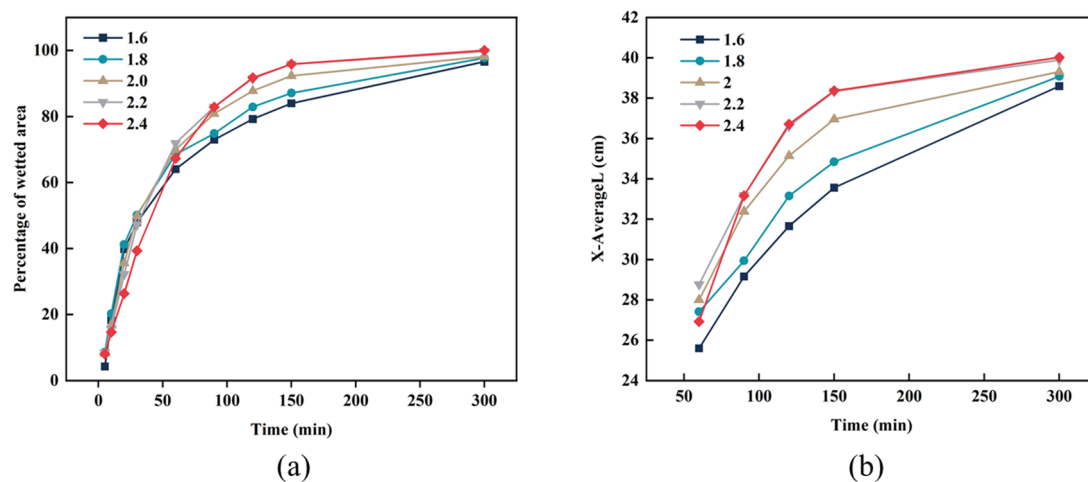


Figure 6. (a) Changes in the percentage of moistened area for different heaps over time. (b) Variation of the average lateral diffusion distance over time for different heaps after 60 min.

In Figure 5, there are some discontinuous wetting phenomena during the first 10 min of heaps with fractal dimensions of 1.6 and 1.8. This indicates that the vertical flow inside heaps with smaller fractal dimensions is more active. However, the fast vertical flow channels do not pass through more areas, which may exacerbate channeling phenomena in heap leaching [24]. Studies have shown that heaps with smaller fractal dimensions have higher porosity, and permeability will exhibit an exponential increase as the fractal dimension decreases [25]. For heaps with larger fractal dimensions, the increased resistance formed by more fine particles will further hinder the flow of liquid under the influence of gravity. To some extent, the slowing of flow within the heap can enhance the reaction

time between the leaching solution and the ore, thereby increasing the reaction efficiency of the heap. However, the overall decrease in flow velocity within the heap will also prolong the residence time of substances in the heap, which may lead to the accumulation of substances and the formation of unfavorable precipitates, such as calcium sulfate. These precipitates can exacerbate pore clogging, leading to deterioration of the heap structure and consequently diminishing the leaching performance of the heap [26].

3.2. Flow Characteristics of Moistened Ore Heap

In the second stage, we obtained fluorescence-subtracted images at different times using the method described earlier, as shown in Figure 7. Similar to the discontinuous wetting phenomena observed in dry ore heaps, the fluorescence-subtracted images of wet ore heaps with fractal dimensions of 1.6 and 1.8 also exhibit numerous black voids. This implies that even below the drip point (in the area near the main flow channel), there are many ore regions with little influence from the flow channels, making it difficult to displace surrounding liquids through convective forms. This also indicates that the diffusion effect formed by concentration gradients has a limited impact on material displacement within the heap. With the increase in fractal dimension, the number of larger black voids in the image decreases, indicating more thorough liquid displacement within the heap. Under the distribution of fractal particles, as the fractal dimension increases, the proportion of medium-sized particles increases, and the capillary channels between particles become more abundant. A uniform and continuous network of capillaries is more conducive to liquid flow within the heap.

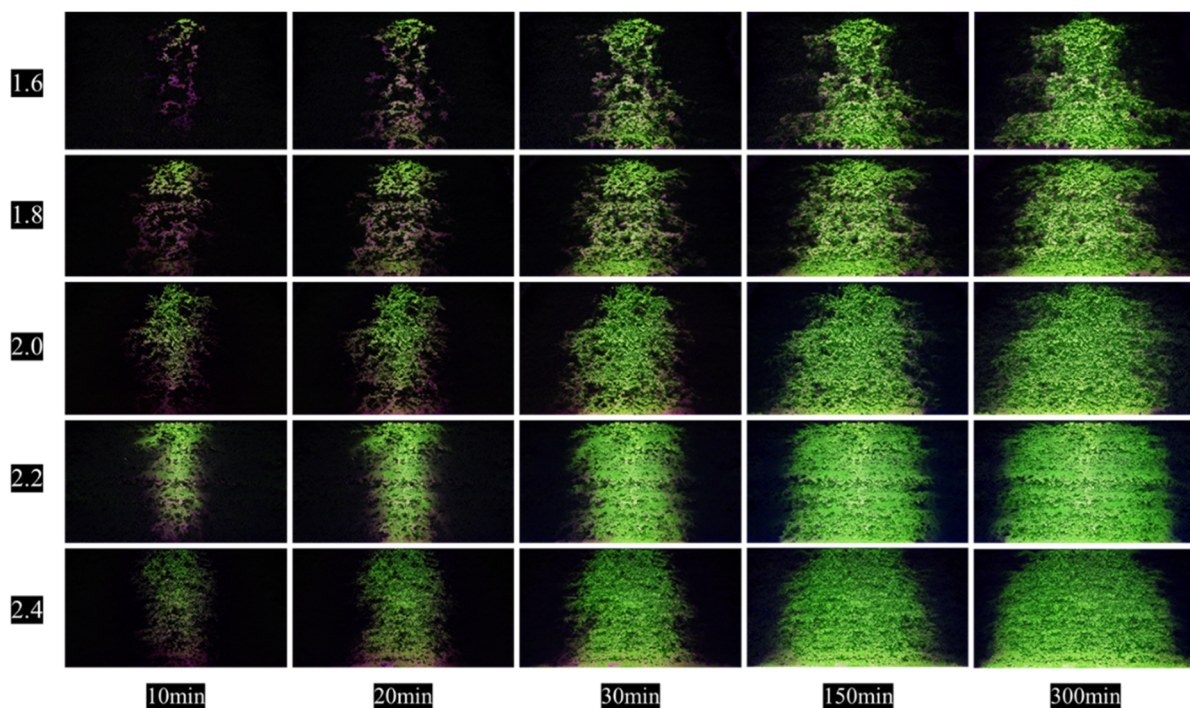


Figure 7. Fluorescence subtraction image of each heap at different time points.

The calculation of the early Y-axis average wetting velocity for dry and wet ore heaps is shown in Figure 8. During the wetting phase of the dry ore heap, the Y-axis seepage velocity slows with increasing fractal dimension, which may lead us to mistakenly believe that in actual production, ore beds with smaller fractal dimensions undergo more active material exchange along the Y-axis. In reality, after wetting the ore bed, heaps with a fractal dimension greater than 1.8 exhibit a significant increase in the Y-axis seepage velocity, indicating that the longitudinal flow of liquid becomes more active after wetting the ore bed. After wetting, internal water channels are established, and water quickly flows

through these channels to the bottom [17,27]. However, the Y-axis seepage velocity of the heap with a fractal dimension of 1.6 does not increase after wetting; it may even decrease. The main reason may be that the pore space between the particles of the ore pile with a small fractal dimension is large, which does not cause resistance to Y-direction seepage in the early stage of seepage in dry deposits, and even the capillary force accelerates its seepage downward, so there is not much difference in the Y-direction seepage rate of the liquid in the dry and wet deposits. The shrinkage of the seepage region toward the center in low-fractal-dimension ore piles is also an important reason for the decrease in apparent Y-direction velocity, which will be further explained in a later section.

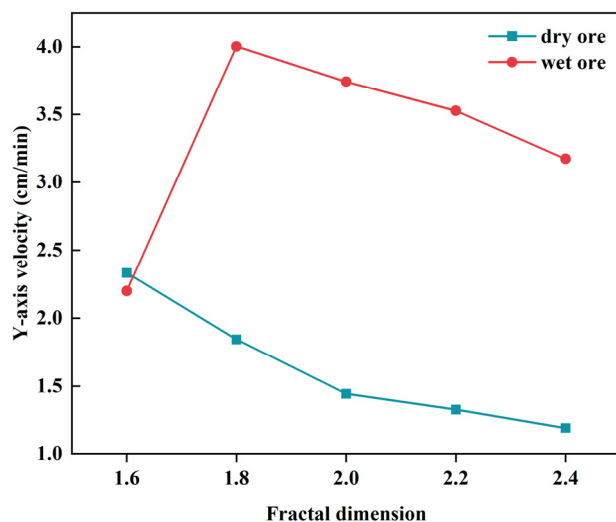


Figure 8. Average Y-axis wetting velocity of each heap in the dry and wet heap states before the flow area reaches the bottom.

3.3. Percolation Area Analysis

Observing all the fluorescence-subtracted images, it was noted that each exhibited two distinct percolation regions with varying fluorescence intensities. For analysis, the green channel image was selected from the fluorescence-subtracted images captured in the second stage at 300 min. Frequency distribution graphs of fluorescence intensity for each heap were then plotted, as illustrated in Figure 9.

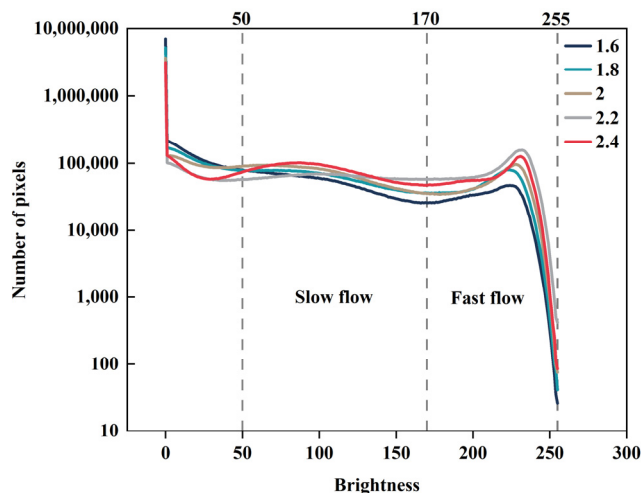


Figure 9. Frequency distribution of fluorescence intensity in the fluorescence-subtracted images for each heap after the second 300 min.

According to the results of image adjustment, the fluorescence intensity reaches 50, which clearly distinguishes the boundary between the flow region and the nonflow region. When the fluorescence intensity reaches 170, the frequency valleys, along with the presence of strong peaks and gentle peaks on both sides, suggest the existence of two distinct regions with different fluorescence intensities in the image. This information can be utilized to delineate boundaries between different flow regions. By employing a threshold of 50 for segmentation and binarization of the fluorescence-subtracted green channel image, the flowing and nonflowing regions can be successfully differentiated. Similarly, using a threshold of 170 on the flowing region subdivides it into fast- and slow-flow regions. The processing results are shown in Figure 10. These findings indicate that the threshold segmentation method based on frequency distribution graphs is effective at identifying different percolation regions [28,29].

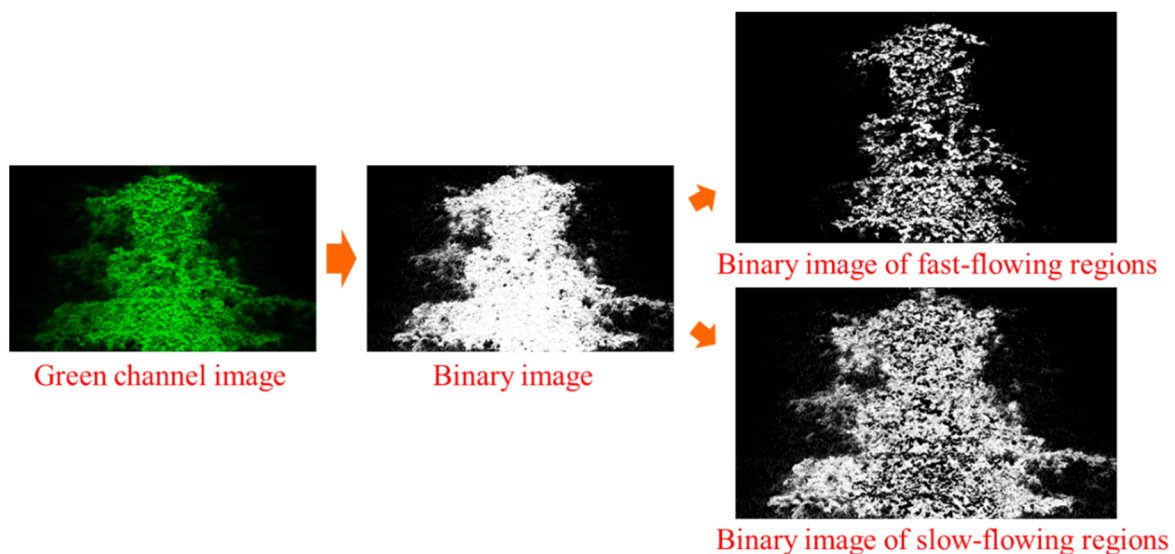


Figure 10. Schematic of threshold segmentation of the fluorescence-subtracted image of a heap with a fractal dimension of 1.6 at the second 300 min.

For all heaps, threshold segmentation and binarization were applied to the fluorescence images from the first 300 min and the fluorescence-subtracted images from the latter 300 min, using an intensity threshold of 50. The mean gray value (mean gray value = integrated density/area) was then calculated for each, representing the size of the active region. A higher mean gray value closer to 255 indicates a larger active area. The percentage of the flowing area in the wet region of the heap during the latter 300 min relative to the wet region of the dry heap at 300 min is also presented in Figure 11a as a line graph.

The average gray values for the first 300 min correspond to the size of the wet region in the dry heap. Due to the combined effects of intraparticle capillaries and interparticle capillaries, as the fractal dimension increases, the liquid can diffuse over a wider range, corresponding to the analysis in Figure 5. The flow in the latter 300 min occurs within the wet heap. The difference in the size of the flowing area before and after indicates that the initial wet region cannot fully represent the entire percolation process of the heap. After the establishment of the wet area, the actual seepage area within the heap is smaller than the wetted area [19], and there is a significant gap. The percolation area of the heap reaches a plateau when the fractal dimension reaches 2.2 and even slightly decreases at 2.4, suggesting that the promoting effect of the fractal dimension on the percolation area is limited. Although abundant capillaries provide sufficient channels for liquid flow, it is essential to note that with an increase in fine particles, the hindering effect of capillaries on percolation becomes apparent. The proportion of the percolation area decreases with decreasing fractal dimension, indicating that, after wetting, percolation in heaps with

smaller fractal dimensions tends to be more concentrated and may more easily establish dominance in flow.

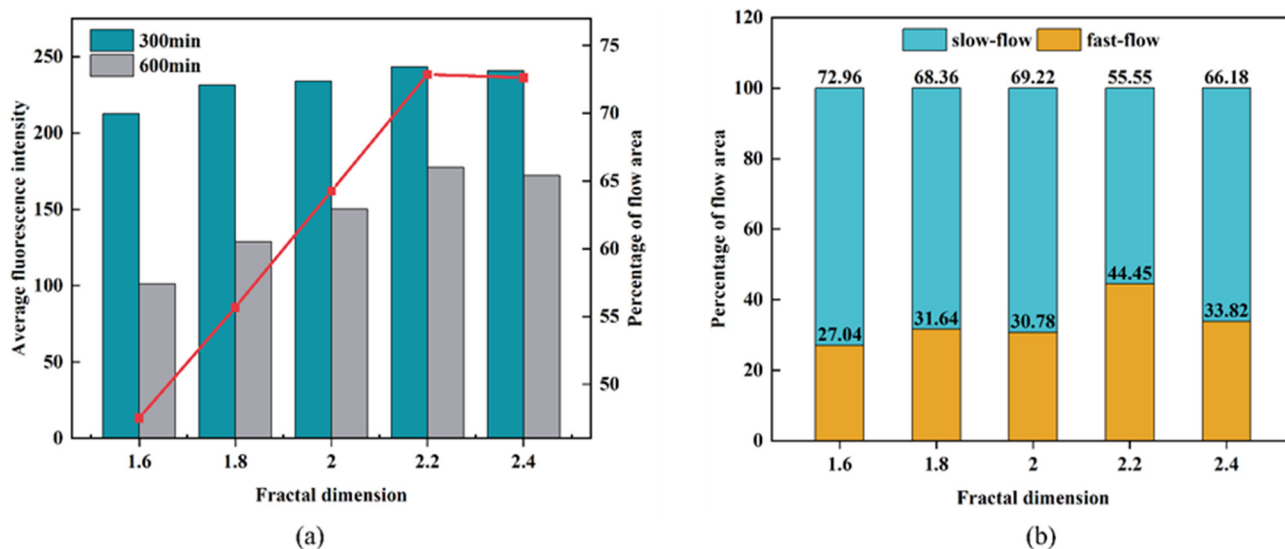


Figure 11. Plants of the size of the wetted and flowing areas (left Y-axis) and the percentage of flowing areas (right Y-axis) for different heaps (a) and the percentage of the total flowing area accounted for by the fast- and slow-flowing areas for each heap at the 600th min (b).

The proportion of the fast-flowing region within the actual flowing area is a key aspect that deserves attention. Figure 11b indicates that the proportion of fast-flowing areas in all heaps is approximately 30%. Among them, the heap with a fractal dimension of 1.6 provides the smallest proportion of fast percolation areas, and at the same time, it has the smallest total percolation area, indicating a significant concentration of percolation within. The heap with a fractal dimension of 2.2 simultaneously possesses the largest proportion of fast-flowing areas and the largest total flowing area, implying more uniform percolation. This suggests that a well-controlled heap particle size distribution can achieve a balance between the internal capillary effects and ore resistance, thereby enhancing the percolation performance of the heap.

3.4. Flow Channels in Ore Heap

Figure 12 shows the outflow at the various drainage outlets at the different time intervals. Initially, from an overall perspective, as the fractal dimension of the particle size distribution increases, the number of drainage outlets with water discharge gradually increases. This implies a significant increase in the number of flow pathways within the heap that can generate water flow, corresponding to the earlier discussion on the increase in convection regions within the heap with the increase in fractal dimension. Examining the drainage situation in Figure 12a, it is observed that during the first 300 min of irrigation, two streams with equal discharge emerged above drainage outlets 1 and 0. As time progresses, the flow channels gradually converge toward outlet 0. By combining this information with the low proportion of the percolation area in low fractal dimension heaps, as shown in Figure 11b, it is evident that percolation in heaps with low fractal dimensions tends to favor the development of dominant flow. This can be attributed to two main reasons: first, in heaps with low fractal dimensions, there are many larger interparticle voids, which significantly reduce the resistance to vertical flow, making it less obstructive for streams to split as they flow downward; second, oversized voids result in the discontinuity of capillaries, weakening the effectiveness of channels guiding lateral flow. Anyway, the trend of percolation within the heap developing toward the formation of a larger dominant flow is evidently unfavorable for heap leaching [30].

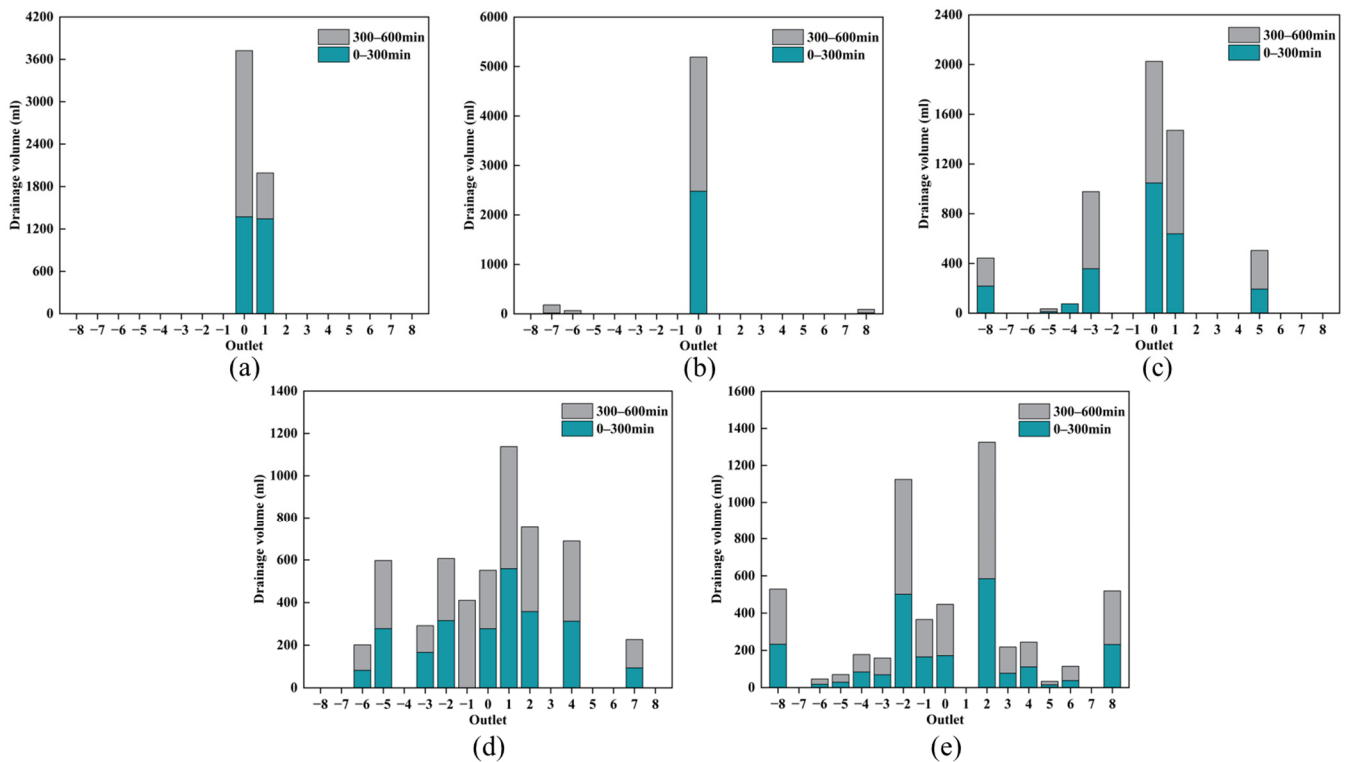


Figure 12. Water discharge capacity from drainage outlets of heaps with particle size distribution fractal dimensions of 1.6–2.4 (a–e).

It should be noted that in Figure 7 the fluorescence-subtracted images of the fractal dimensions of 1.6 and 1.8 mine stacks indicate the presence of wider lateral seepage areas during drip irrigation, whereas Figure 12a,b show very few drains at the bottom of both. Typically, multiple drain openings under the flow region should experience fluid draining out, but this is not the case. This suggests that in low-fractal heaps, the transverse seepage relies mainly on the flow of a thin film of water transverse to the surface of the particles [31]. When the fractal dimension of the heap is greater than 2, the number of drainage outlets for water increases, suggesting that laterally split gravity flow paths are more likely to occur in piles with high fractal dimensions.

After the fractal dimension exceeds 1.8, the water discharge from most outlets during 0–300 min and 300–600 min was generally consistent. It indicates that during the initial stage of infiltration, a stable flow channel has already formed inside the heap. Examining the total water discharge from each outlet at 600 min, although the heap with a fractal dimension of 2.4 has the highest number of outlets with water flow, the main outlets are still occupied by -2 , $+2$, -8 , and $+8$. This phenomenon suggests a concentration of flow in smaller channels, indicating that, with an increase in the proportion of fine particles to a certain extent, uneven percolation may occur due to the increased resistance of ore particle obstruction. In contrast, the water discharge from each outlet at 2.2 is relatively uniform. In heap leaching operations, percolation with a fractal dimension of 2.2 appears to be more ideal, as the differences in water discharge among various outlets are small. This suggests the possible formation of multiple fast percolation channels evenly distributed within the heap, with similar flow rates. This finding aligns with the maximum performance of fast flow areas at a fractal dimension of 2.2 in Figure 11b, demonstrating the practicality of fluorescence-subtracted image analysis.

4. Conclusions

This study utilized the UV fluorescence labeling method to visualize the leaching process in heaps with different fractal gradations. Unlike previous experimental designs with

UV fluorescence labeling, we employed a new form of fluorescence image acquisition and analysis methods, obtaining more information about the leaching process in fluorescence images. Using this approach, we investigated the common occurrence of fractal gradations in heap leaching production, providing further insights into the impact of gradation on leaching in practical production.

The results indicate that using fluorescence-subtracted images can more accurately characterize the internal flow areas within the heap. Further analysis of these fluorescence-subtracted images allows for the quantification of flow areas, breaking them down into fast-flow and slow-flow regions, enabling researchers to gain a deeper understanding of internal flow processes.

According to the results of percolation with fractal grading, after wetting the ore bed, longitudinal flow within the heap becomes more active. Heaps with smaller fractal dimensions exhibit more blind spots in flow. To some extent, percolation zones increase with increasing fractal dimension. Concentration gradients have a limited impact on material exchange within the heap, where material exchange primarily relies on lateral percolation and longitudinal splitting flow. In heaps with lower fractal grading, lateral percolation primarily depends on a thin layer of water film flowing on particle surfaces. In heaps with higher fractal grading, the primary mechanism for lateral percolation relies on lateral splitting facilitated by longitudinal channels. Excessively increasing the fractal dimension of grading does not lead to a more even distribution of percolation within the heap. At a fractal dimension of 2.4, a phenomenon of concentrated dominant flow reappears. In summary, under ideal conditions without considering structural changes due to chemical erosion or uneven stacking, the pore structure formed by a fractal grading dimension of 2.2 is more suitable for heap leaching.

In this work, we have proposed a novel method for studying percolation, which will greatly facilitate subsequent research on heap leaching. It is important to note that the experimental results can serve as a reference for the percolation in non-agglomerated heaps. However, due to differences in parameters such as wettability and particle porosity in specific ore bodies, the percolation results obtained may vary slightly.

Author Contributions: Conceptualization, Y.Z. and J.W.; methodology, X.W.; validation, X.W. and J.H.; formal analysis, X.W. and M.G.; investigation, X.W. and X.L.; resources, J.W. and Y.Z.; data curation, X.W. and W.Y.; writing, X.W.; supervision, H.L.; funding acquisition, Y.Z. All authors have read and agreed to the published version of the manuscript.

Funding: This research was funded by The National Key Research and Development Program of China (grant number: 2022YFC2105303) and The National Nature Science Foundation of China (grant number: 51974363).

Data Availability Statement: Data are contained within the article.

Conflicts of Interest: The authors declare no conflicts of interest.

References

1. Oxley, A.; Smith, M.E.; Caceres, O. Why heap leach nickel laterites? *Miner. Eng.* **2016**, *88*, 53–60. [[CrossRef](#)]
2. Petersen, J. Heap leaching as a key technology for recovery of values from low-grade ores—A brief overview. *Hydrometallurgy* **2016**, *165*, 206–212. [[CrossRef](#)]
3. Ghorbani, Y.; Franzidis, J.-P.; Petersen, J. Heap Leaching Technology—Current State, Innovations, and Future Directions: A Review. *Miner. Process. Extr. Metall. Rev.* **2016**, *37*, 73–119. [[CrossRef](#)]
4. Wang, L.-M.; Yin, S.-H.; Wu, A.-X. Visualization of flow behavior in ore-segregated packed beds with fine interlayers. *Int. J. Miner. Metall. Mater.* **2020**, *27*, 900–909. [[CrossRef](#)]
5. Ilankoon, I.; Neethling, S. The effect of particle porosity on liquid holdup in heap leaching. *Miner. Eng.* **2013**, *45*, 73–80. [[CrossRef](#)]
6. Yang, B.-H.; Wu, A.-X.; Jiang, H.-C.; Chen, X.-S. Evolution of permeability of ore granular media during heap leaching based on image analysis. *Trans. Nonferrous Met. Soc. China* **2008**, *18*, 426–431. [[CrossRef](#)]
7. Zhang, S.; Liu, W.; Granata, G. Effects of grain size gradation on the porosity of packed heap leach beds. *Hydrometallurgy* **2018**, *179*, 238–244. [[CrossRef](#)]
8. Ghorbani, Y.; Becker, M.; Mainza, A.; Franzidis, J.-P.; Petersen, J. Large particle effects in chemical/biochemical heap leach processes—A review. *Miner. Eng.* **2011**, *24*, 1172–1184. [[CrossRef](#)]

9. Zhang, J.; Li, M.; Liu, Z.; Zhou, N. Fractal characteristics of crushed particles of coal gangue under compaction. *Powder Technol.* **2017**, *305*, 12–18. [[CrossRef](#)]
10. Moradi, I.; Irannajad, M. Fractal dimension of crushing products: Effects of feed size distribution and feed rate. *Part. Sci. Technol.* **2021**, *39*, 877–886. [[CrossRef](#)]
11. Mandelbrot, B.B.; Mandelbrot, B.B. *The Fractal Geometry of Nature*; WH Freeman: New York, NY, USA, 1982; Volume 1.
12. Tyler, S.W.; Wheatcraft, S.W. Fractal scaling of soil particle-size distributions: Analysis and limitations. *Soil Sci. Soc. Am. J.* **1992**, *56*, 362–369. [[CrossRef](#)]
13. Ding, D.-X.; Fu, H.-Y.; Ye, Y.-J.; Hu, N.; Li, G.-Y.; Song, J.-B.; Wang, Y.-D. A fractal kinetic model for heap leaching of uranium ore with fractal dimension of varied particle size distribution. *Hydrometallurgy* **2013**, *136*, 85–92. [[CrossRef](#)]
14. Turcotte, D.L. Fractals and fragmentation. *J. Geophys. Res. Solid Earth* **1986**, *91*, 1921–1926. [[CrossRef](#)]
15. Ilankoon, I.; Neethling, S. Liquid spread mechanisms in packed beds and heaps. The separation of length and time scales due to particle porosity. *Miner. Eng.* **2016**, *86*, 130–139. [[CrossRef](#)]
16. Xue, Z.; Gan, D.; Zhang, Y.; Liu, Z.; Duan, X.; Huang, M. Liquid spread mechanisms in high-temperature underground stope leaching. *Miner. Eng.* **2020**, *156*, 106497. [[CrossRef](#)]
17. Fagan, M.A.; Ngoma, I.E.; Chieme, R.A.; Minnaar, S.; Sederman, A.J.; Johns, M.L.; Harrison, S.T. MRI and gravimetric studies of hydrology in drip irrigated heaps and its effect on the propagation of bioleaching micro-organisms. *Hydrometallurgy* **2014**, *150*, 210–221. [[CrossRef](#)]
18. Fernando, W.A.M.; Ilankoon, I.; Rabbani, A.; Chong, M.N. Applicability of pore networks to evaluate the inter-particle flow in heap leaching. *Hydrometallurgy* **2020**, *197*, 105451. [[CrossRef](#)]
19. Ilankoon, I.; Neethling, S. Inter-particle liquid spread pertaining to heap leaching using UV fluorescence based image analysis. *Hydrometallurgy* **2019**, *183*, 175–185. [[CrossRef](#)]
20. Citarella, D.; Cupola, F.; Tanda, M.G.; Zanini, A. Evaluation of dispersivity coefficients by means of a laboratory image analysis. *J. Contam. Hydrol.* **2015**, *172*, 10–23. [[CrossRef](#)]
21. Yin, S.-H.; Wang, L.-M.; Xun, C.; Wu, A.-X. Effect of ore size and heap porosity on capillary process inside leaching heap. *Trans. Nonferrous Met. Soc. China* **2016**, *26*, 835–841. [[CrossRef](#)]
22. Odidi, M.D.; Fagan-Endres, M.A.; Harrison, S.T.L. Moisture absorption rates via capillary suction within packed beds—The effect of material and fluid properties with implications for heap leaching operations. *Hydrometallurgy* **2023**, *215*, 105975. [[CrossRef](#)]
23. Bouffard, S.C.; Dixon, D.G. Investigative study into the hydrodynamics of heap leaching processes. *Metall. Mater. Trans. B* **2001**, *32*, 763–776. [[CrossRef](#)]
24. Wu, A.; Yin, S.; Yang, B.; Wang, J.; Qiu, G. Study on preferential flow in dump leaching of low-grade ores. *Hydrometallurgy* **2007**, *87*, 124–132. [[CrossRef](#)]
25. Chen, Y.; Yu, B.; Zhang, K.; Zhang, M.; Xu, G.; Chen, Z. Permeability evolution and particle size distribution of saturated crushed sandstone under compression. *Geofluids* **2018**, *2018*, 6043420. [[CrossRef](#)]
26. Wu, A.X.; Yao, G.H.; Huang, M.Q. Influence factors of permeability during heap leaching of complex copper oxide ore. *Adv. Mater. Res.* **2012**, *347*, 1037–1043. [[CrossRef](#)]
27. Dixon, D.G. Heap leach modeling—the current state of the art. *Hydrometallurgy* **2003**, *1*, 289–314.
28. Raju, P.D.R.; Neelima, G. Image segmentation by using histogram thresholding. *Int. J. Comput. Sci. Eng. Technol.* **2012**, *2*, 776–779.
29. Tobias, O.J.; Seara, R. Image segmentation by histogram thresholding using fuzzy sets. *IEEE Trans. Image Process.* **2002**, *11*, 1457–1465. [[CrossRef](#)] [[PubMed](#)]
30. Eriksson, N.; Destouni, G. Combined effects of dissolution kinetics, secondary mineral precipitation, and preferential flow on copper leaching from mining waste rock. *Water Resour. Res.* **1997**, *33*, 471–483. [[CrossRef](#)]
31. Tokunaga, T.K.; Wan, J. Water film flow along fracture surfaces of porous rock. *Water Resour. Res.* **1997**, *33*, 1287–1295. [[CrossRef](#)]

Disclaimer/Publisher’s Note: The statements, opinions and data contained in all publications are solely those of the individual author(s) and contributor(s) and not of MDPI and/or the editor(s). MDPI and/or the editor(s) disclaim responsibility for any injury to people or property resulting from any ideas, methods, instructions or products referred to in the content.